nature communications

Article

https://doi.org/10.1038/s41467-025-56000-y

# An unusual chiral-at-metal mechanism for BINOL-metal asymmetric catalysis

Received: 12 July 2024

Accepted: 6 January 2025

Published online: 16 January 2025

Check for updates

Zhenxing Li[1], Pengfei Chen[2], Zhigang Ni[3], Liuzhou Gao[4], Yue Zhao[5], Ranran Wang[6], Congqing Zhu[2], Guoqiang Wang[1] ✉ & Shuhua Li[1] ✉

Chiral binaphthols (BINOL)-metal combinations serve as powerful catalysts in asymmetric synthesis. Their chiral induction mode, however, typically relies on multifarious non-covalent interactions between the substrate and the BINOL ligand. In this work, we demonstrate that the chiral-at-metal stereoinduction mode could serve as an alternative mechanism for BINOL-metal catalysis, based on mechanistic studies of BINOL-aluminum-catalyzed asymmetric hydroboration of heteroaryl ketones. Theoretical calculations reveal that an octahedral stereogenic-at-metal aluminum alkoxide species is the most stable species within the reaction system, and also is the catalytic relevant intermediate, promoting the stereo-determining hydroboration reaction through a ligand-assisted hydride transfer mechanism rather than the conventional hydroalumination mechanism. These computations reproduce the experimental selectivities and also rationalize the stereoinduction mechanism, which arises from the aluminum-centered chirality induced by chiral BINOL ligands during diastereoselective assembly. The reliability of the proposed mechanism could be verified by the single-crystal X-ray diffraction characterization of the octahedral aluminum alkoxide complex. Additional NMR and Electronic Circular Dichroism (ECD) experiments elucidated the behavior of the hexacoordinated aluminum alkoxide in the solution phase. We anticipate that these findings will extend the applicability of BINOL-metal catalysis to a broader range of reactions.

Asymmetric catalysis provides a powerful tool for the precise construction of multi-level chiral functional materials[1–3]. Understanding the chiral induction mechanism is one of the central questions in the area of asymmetric synthesis[4–6], and it is of great significance for the rational design of catalysts producing improved stereoselectivity and even novel catalytic strategies[7–10]. Chiral binaphthols (BINOL)-metal complexes, with their expansive combinatorial possibilities and exceptional chiral control capabilities, have become powerful catalysts in asymmetric synthesis[11–14]. Over the past few decades, a wide range of asymmetric reactions have been developed utilizing BINOL-metal combinations. Despite the diverse applications of BINOL ligands, the chiral induction mechanism of these processes mainly relies on non-

[1]State Key Laboratory of Coordination Chemistry, Key Laboratory of Mesoscopic Chemistry of Ministry of Education, School of Chemistry and Chemical Engineering, Nanjing University, Nanjing, China. [2]State Key Laboratory of Coordination Chemistry, Jiangsu Key Laboratory of Advanced Organic Materials, School of Chemistry and Chemical Engineering, Nanjing University, Nanjing, China. [3]College of Material, Chemistry and Chemical Engineering, Key Laboratory of Organosilicon Chemistry and Material Technology of Ministry of Education, Hangzhou Normal University, Hangzhou, China. [4]School of Chemistry and Chemical Engineering, Yangzhou University, Yangzhou, China. [5]State Key Laboratory of Coordination Chemistry, Chemistry and Biomedicine Innovation Center (ChemBIC), School of Chemistry and Chemical Engineering, Nanjing University, Nanjing, China. [6]State Key Laboratory of Analytical Chemistry for Life Science, Jiangsu Key Laboratory of Advanced Organic Materials, School of Chemistry and Chemical Engineering, Nanjing University, Nanjing, China. ✉e-mail: wangguoqiang710@nju.edu.cn; shuhua@nju.edu.cn

covalent interactions[15,16] between the catalyst microenvironment and the substrates (Fig. 1a).

Stereospecific catalytic hydroboration of ketones is one of the most efficient methods to generate chiral alcohols that are fundamental functionalities in pharmaceuticals, natural products, etc[17,18]. This can be achieved by either transition metal[19–21] or rare-earth metal catalysis[22–24]. The use of main-group element catalysts for the hydroboration of carbonyl derivatives is highly attractive due to the advantages of economy and environmental sustainability[25–28]. In this field, aluminum[29–32], calcium[33,34], magnesium[35,36], and boron catalysts[37] have been reported. Despite these achievements, examples of enantioselective hydroboration of ketones with main-group catalysts are still rare[38–41]. Recently, Rueping and coworkers elegantly introduced a BINOL-aluminum catalytic system for the asymmetric hydroboration of heteroaryl ketones **1** using pinacolborane (HBpin) (Fig. 1b)[42]. A pathway involving the hydroalumination of C=O bond was proposed for this borylation reaction. It is speculated that the hydroalumination step is the stereo-determining step, with the steric hindrance effect being the source of enantioselectivity (Fig. 1b). It should be mentioned that such a BINOL-aluminum catalytic system is not only applicable to

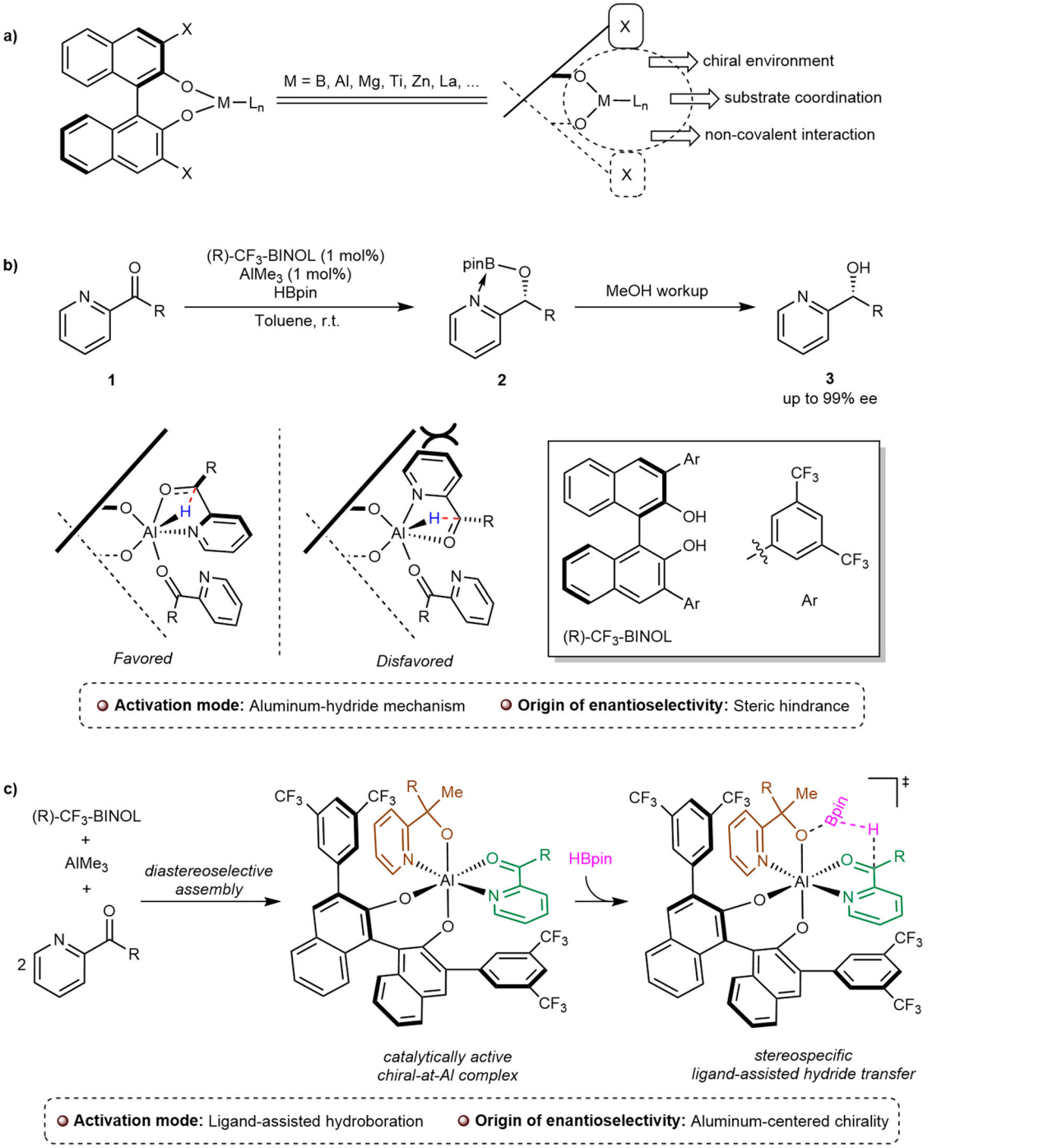


**Fig. 1 | BINOL-metal catalysts. a** Schematic representation of BINOL-metal catalysts, basic activation mode and chiral induction mechanism. **b** Asymmetric hydroboration of heteroaryl ketones by BINOL-aluminum catalysis and previously proposed aluminum hydride-based mechanism. **c** Unlocking octahedral chiral-at-metal catalysis mechanism in BINOL-metal catalytic systems with BINOL-aluminum-catalyzed asymmetric hydroboration of heteroaryl ketones as a case of study (This work).

the alkyl-(pyridine-2-yl) methanones but also suitable to aryl-(pyridine-2-yl) methanones, a type of substrate with low discrimination in terms of steric hindrance between the two substituents at the carbonyl carbon atom. This distinctive reaction outcome intrigued us to revisit the rationale of this asymmetric hydroboration of heteroaryl ketones.

In this work, by employing a combination of quantum chemical calculations and experimental studies on the mechanism of BINOL-aluminum-catalyzed asymmetric hydroboration of heteroaryl ketones, an unusual octahedral chiral-at-aluminum complex[43–47], resulting from BINOL ligands-induced diastereoselective assembly, was discovered (Fig. 1c). This aluminum complex is predicted to be thermodynamically more favorable than the previously proposed aluminum hydride complex, being the real catalytically relevant species. The proposed octahedral aluminum alkoxide complex was isolated and characterized by single-crystal X-ray diffraction analysis, NMR and ECD spectra. Additionally, this isolated aluminum species has been proven to reproduce the reactivity of the in situ generated catalyst. With this hexacoordinated aluminum alkoxide complex as the key intermediate, a different pathway involving a sequence of ligand-assisted hydride transfer[48,49], Al-O/O-B σ-bond metathesis, was proposed. Ligand-assisted hydroboration of octahedral chiral-at-aluminum complex with HBpin is the stereo-determining step. The source of enantioselectivity is the aluminum-centered chirality rather than steric repulsion. The discovered chiral induction mode could account for the observed enantioselectivity of both alkyl-(pyridine-2-yl) methanones and aryl-(pyridine-2-yl) methanones. To the best of our knowledge, this chiral-at-aluminum catalytic mechanism represents a pioneering metal-centered stereoinduction mode in the field of BINOL-metal catalysis.

## Results

### Theoretical investigations on possible BINOL-Al complex within the catalytic system

Based on previous studies on aluminum-catalyzed asymmetric Meerwein-Schmidt-Ponndorf-Verley reduction of ketones[15,50–52], we first explored two pathways leading to different catalytically active species: the aluminum hydride (Al-H) and the aluminum alkoxide (Fig. 2a) with B3LYP[53,54]-D3[55] calculations. Optimized structures were obtained at Def2-SVP basis set, and single-point calculations were conducted at a large Def2-TZVP basis set. The solvent effect was treated with Polarizable Continuum Model (PCM)[56,57] (toluene). Since [(R)-$CF_3$-BINOL-AlMe]$_2$ **4-dimer** has already been experimentally characterized[42], we use **4-dimer** as the starting point of the free energy profile and 2-acetylpyridine **1a** as the model substrate.

Figure 2a displays the computed free energy profile for the formation of both the previously reported aluminum hydride species and the discovered hexacoordinated aluminum alkoxide complexes. In line with earlier studies by Rueping et al., the formation of the aluminum hydride species follows a sequential process involving methyl migration and Al-O/H-B σ-bond metathesis (Fig. 2a, in gray line)[42]. This process is exergonic by 22.9 kcal/mol, and the methyl migration step is the rate-limiting step with an activation barrier of 21.9 kcal/mol (via **TS-6-7**). While this process is kinetically accessible, we unexpectedly observed that for the pentacoordinated intermediate **7**, the nitrogen atom of the coordinated 2-acetylpyridine **1a** can further bind with the aluminum center, leading to the formation of hexacoordinated aluminum alkoxides, such as **12c** and **12f** (Fig. 2a, in blue line). In both **12c** and **12f**, substrate **1a** exhibits a bidentate coordination mode with the aluminum center. The formation of these two species is notably exergonic, with energy releases of 49.5 and 44.2 kcal/mol, respectively. It is worth noting that the previously mentioned aluminum hydride intermediate **10** is predicted to be thermodynamically less favorable than **12c** by a substantial margin, with an energy difference of 26.6 kcal/mol. Also, hexcoordinated aluminum alkoxides are more stable than pentacoordinated aluminum alkoxides (Supplementary Figs. 2 and 4). It shoud also be mentioned that we also computationally revisited the hydroboration reaction with 2-benzoylpyridine as the model substrate. We found that the aluminum hydride mechanism failed to explain the stereoselectivity when using 2-benzoylpyridine as the model substrate according to the small barrier difference ($\Delta\Delta G^{\ddagger}_{cal}$ = 0.2 kcal/mol), which is in contradiction with the experimentally observed enantioselectivity (98% ee, $\Delta\Delta G^{\ddagger}_{exp}$ > 2.7 kcal/mol) (Supplementary Fig. 3). These results hint that the stereoselective hydroboration of heteroaryl ketones via the aluminum hydride mechanism is unlikely.

Along with **12c** and **12f**, eight configurations of hexacoordinated aluminum alkoxides could be located through ligand rearrangement, and all of them possess metal-centered chirality (Fig. 2b)[47,58]. Among these configurations, **12c** is the most stable species. The free energy difference of the second most stable species **12g** relative to **12c** is as high as 4.5 kcal/mol. To validate the reliability of B3LYP-D3 calculations, we conducted a benchmark study using highly accurate DLPNO-CCSD(T)[59] method (Supplementary Table 2). The absolute errors between the B3LYP-D3 and DLPNO-CCSD(T) relative energies are always less than 1.0 kcal/mol, highlighting the reliability of B3LYP-D3 results. This means that BINOL-AlMe reacts with two equivalents of heteroaryl ketone substrates, leading to a chiral-at-metal complex with a definite stereo configuration such as **12c** in this system. In this complex, the substrate with bidentate coordination at the metal center is in a well-defined chiral environment, which facilitates the following asymmetric transformation.

Previously, the generation of chiral-at-metal catalysts typically required the use of transition metals or multidentate ligands[43–47]. This BINOL-induced asymmetric self-assembly provides an alternative route to generate chiral-at-metal complexes. Two factors, π-π stacking[60,61] and trans-effect[62,63] might be responsible for the unique stability of **12c**. Generally, Λ-configured aluminum species feature better π-π stacking interactions than Δ-configurations (Supplementary Fig. 6). As displayed in Fig. 2c, both two side arms of the BINOL ligand in **Λ-12c** adopt π-π stacking interactions with the coordinated substrates. Besides, the two pyridine groups in **12c** adopted in trans-orientation can avoid the trans-effect of the pyridine ligands with strong σ-donors (here are the BINOLate, alkoxide, etc.), which might weaken the coordination of pyridine groups. This trans-effect is supported by the shorter Al-N bond distances in **Λ-12c** (2.02 Å and 2.06 Å) than the other seven configurations ($d_{Al\text{-}N}$ = 2.03 - 2.22 Å) (Supplementary Table 1). These two factors can be used to predict the configuration of other chiral-at-metal complexes.

### Experimental investigation

Based on the comprehensive investigation of possible BINOL-Al complexes within the catalytic system, we speculated that thermodynamically stable hexacoordinated aluminum alkoxides might be experimentally characterized. After extensive screening of the substrate and solvent system, we successfully isolated a hexacoordinated aluminum alkoxides species (**13g**) from the reaction of in situ [(R)-$CF_3$-BINOL-AlMe]$_2$ **4-dimer** with 2-(4-chlorobenzoyl)pyridine **1c** (Fig. 3a).

The solid-state structure of **13g** revealed an octahedral aluminum center with the substrate **1c** bound in a bidentate coordination fashion (Fig. 3a). To investigate other configurational isomers of **13g** in the solvent phase, we performed B3LYP-D3 calculations using the basis sets described above. In these calculations, dichloromethane was used as the solvent within the PCM model. Our computational results showed that **13c, 13f**, and **13g** are more stable than other isomers, and the energy differences of these three structures are within 1.0 kcal/mol (Fig. 3b). The preference for **13g** in the solid state could be attributed to the packing effects and/or solubility difference during the crystallization. Dissolving the crystals of **13g** in deuterated dichloromethane resulted in a complex mixture according to NMR spectra (Supplementary Figs. 18–20). These results indicate that some configurations

https://doi.org/10.1038/s41467-025-56000-y

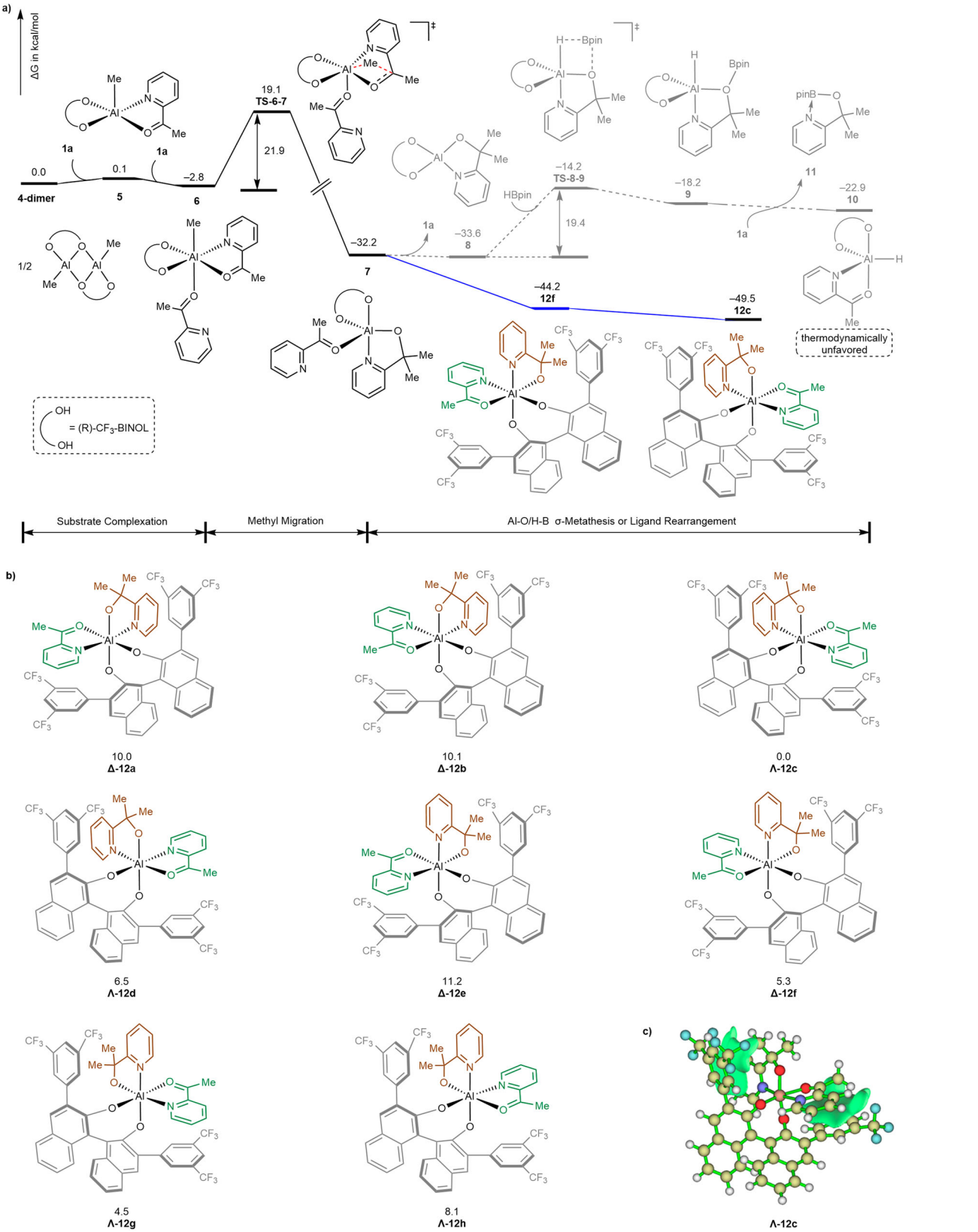


**Fig. 2 | Catalytically active species. a** Reaction pathways for the generation of the aluminum hydride and the hexacoordinated aluminum alkoxide (free energies are with respect to **4-dimer** in kcal/mol). **b** Schematic representations of all diastereomers of hexacoordinated aluminum alkoxides **12** (free energies are with respect to **12c** in kcal/mol). Computational details are described in the text. **c** π-π stacking interaction in **12c** identified by the independent gradient model (IGM)[60,61]. Color codes: H, white; C, yellowish-brown; O, red; N, blue; F, cyan; Al, dusty red.

https://doi.org/10.1038/s41467-025-56000-y

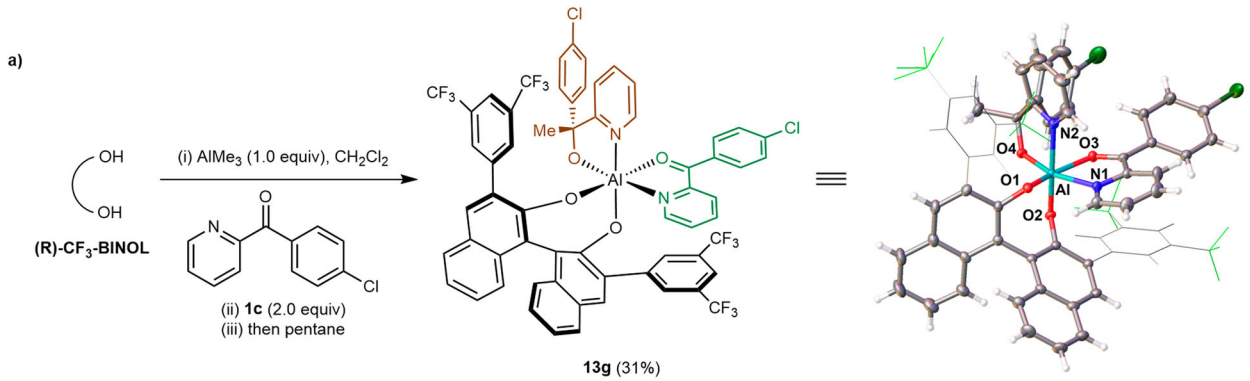


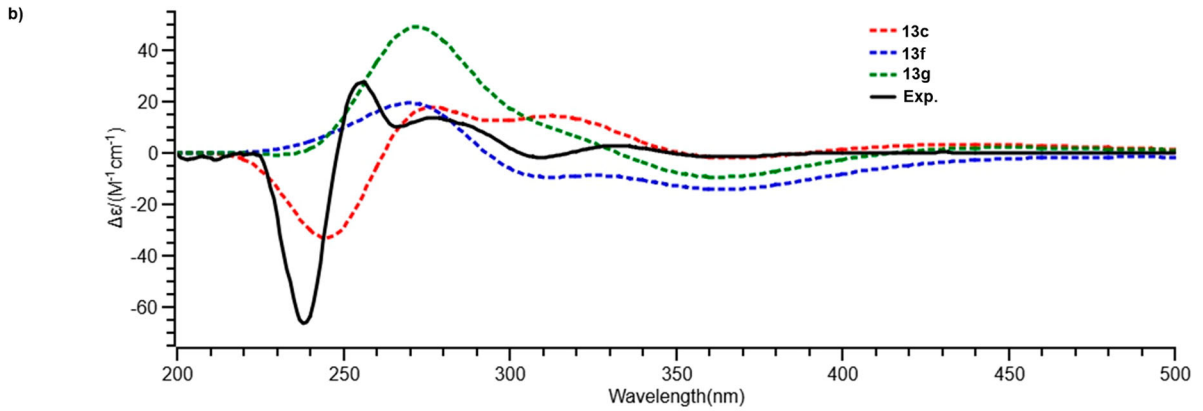


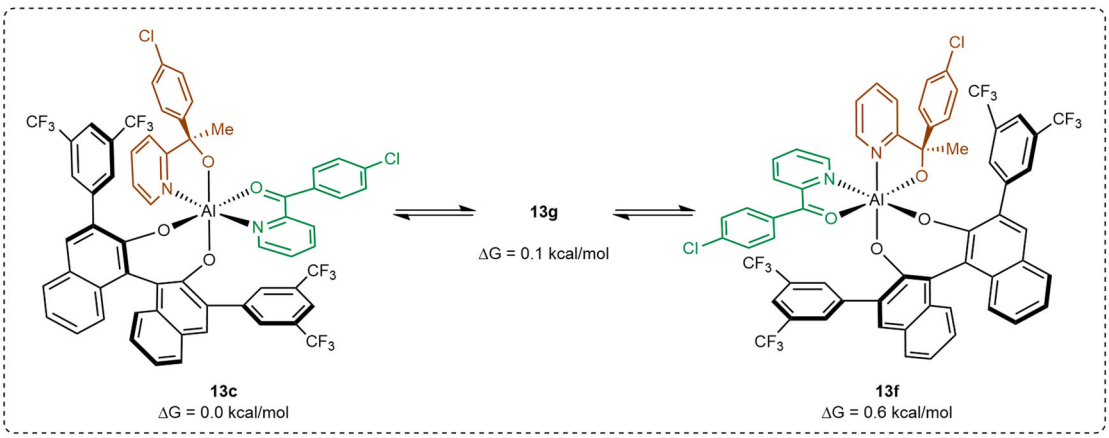


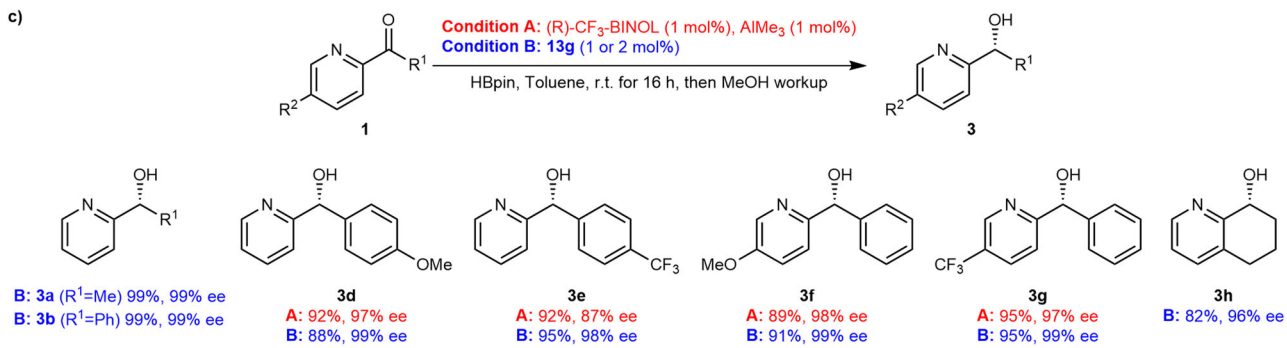


**Fig. 3 | Intermediate isolation and characterization. a** Synthetic route and solid-state structure of a hexacoordinated aluminum alkoxides species **13g**. Color codes: H, white; C, gray; O, red; N, blue; Al, cyan. **b** Experimental and simulated ECD spectra of hexacoordinated aluminum alkoxides species **13** in dichloromethane. Gibbs free energies are in kcal/mol with respect to **13c**. Computational details are described in the text. **c** Catalytic performance validation of hexacoordinated aluminum alkoxides species **13g**. For condition B, only the hydroboration of **1h** was performed with 2 mol% catalyst loading, and the other substrates were reduced with 1 mol% catalyst loading.

of the hexacoordinated aluminum species might coexist and are interconvertible in the solution phase.

To further probe the existing state of the hexacoordinated aluminum species **13g** in the solution phase, ECD investigations were performed (Fig. 3b). The ECD spectrum of the isolated crystals in the dichloromethane solution shows a negative Cotton effect at 238 nm, and a positive Cotton effect at 256 nm and 277 nm (Fig. 3b, black solid line). According to our theoretical calculations, configurations **13c, 13f** and **13g** are the main components in dichloromethane. The simulated ECD spectrum at TD-B3LYP-D3/Def2-TZVP level (with the PCM model, DCM as the solvent) of **13c** (Fig. 3b, red dashed line) shows a negative Cotton effect at 245 nm and a positive Cotton effect at 277 nm and 313 nm, which are qualitatively in accord with experimental results. However, configurations **13f** and **13g** (crystalized configuration) do not contribute to the negative Cotton effect observed at 238 nm but contribute to the positive Cotton effect in the spectrum. We therefore speculated that **13g** in the solid state mainly converts into **13c** in dichloromethane solution. The NMR and ECD experiments demonstrated the substitutional and configurational lability of the BINOL-aluminum complex, which is different from other chiral-at-metal catalysts with configurational inertness.

Subsequently, we investigated the catalytic activity of **13g** using various substrates. As shown in Fig. 3c, both methyl and phenyl substituted substrates **1a** and **1b** reacted with HBpin in the presence of 1 mol% of **13g** with excellent yields and enantioselectivities. **13g** reproduced the reactivity of the in situ generated catalyst[42]. We further validated the catalytic performance of both the in situ generated catalyst and isolated species **13g** using heteroaryl ketones bearing electron-donating or electron-withdrawing groups (Fig. 3c). Our results show that the in situ generated catalyst provided excellent enantioselectivity (97%-98% ee) for heteroaryl ketones **1d** and **1f** bearing electron-donating groups (OMe) and **1g** bearing an electron-withdrawing group ($CF_3$) on the pyridine ring (Condition A). For **1e**, substrate bearing a trifluoromethyl group on the phenyl ring, a slightly lower enantioselectivity (**3e**, 87% ee) was observed when using the in situ generated catalyst. When using the isolated aluminum species **13g** as the catalyst, excellent enantioselectivity can be observed for all four species (Condition B, 98%-99% ee). Notably, for species **1e**, complex **13g** was able to improve the enantioselectivity (ee value) to 98%, surpassing the results obtained under standard condition (Condition A, 87% ee). Subsequently, for cyclic ketone species **1h**, a lower 86% ee value was reported[42] using the in situ generated catalyst. Our results show that employing 2 mol% of isolated **13g** as catalyst leads to a significantly enhanced ee value (96%). These results indicated that this catalytic system is insensitive to electronic effects, and the octahedral chiral-at-aluminum complex might be the actual catalyst for the asymmetric hydroboration of heteroaryl ketones. The slightly worse performance observed with the in situ generated catalyst may be attributed to the formation of other unidentified aluminum species during the reaction[64,65]. Besides, we also found that neither the in situ generated [(R)-$CF_3$-BINOL-AlMe]$_2$ complex nor the isolated aluminum species **13g** could effectively catalyze the asymmetric hydroboration of acetophenone (Supplementary Fig. 34). Our results demonstrated that the bidentate coordination of 2-pyridyl ketones with the Al center is essential for achieving high enantioselectivity in hydroboration.

### Computed hydroboration pathway with octahedral chiral-at-aluminum as the key intermediate

Based on the computational and experimental results, we proposed that hexacoordinated aluminum alkoxides are the resting state of the catalytical species, and then explored free energy profile for the full catalytic cycle of the hydroboration reaction. The intermediates and transition states were located with the help of combined molecular dynamics and coordinate driving method (MD/CD)[66,67]. Hexacoordinated aluminum alkoxides **12** have amphiphilic structural characteristics, in which the alkoxy anion is nucleophilic and the carbonyl group is electrophilic. Many previous studies proposed ligand-assisted hydroboration[48,49] as a crucial step in hydroboration of ketones. Thus, we envisioned that when the boron atom of HBpin coordinates with the nucleophilic alkoxy anion, the nucleophilicity of hydride will be enhanced, facilitating the hydride transfer to the electrophilic carbonyl group. According to our assumption, only when the Al-alkoxy bond and carbonyl group of **12** adopted a non-planar configuration (c.f., Fig. 2b, **12a-12d**), the related ligand-assisted hydroboration process could occur (Supplementary Fig. 7). Because the configuration of **12a-12d** is specific, these hydride transfer events are stereospecific. More specifically, hydride transfer through **12a** or **12d** could only lead to (S)-enantiomers, while hydride transfer through **12b** or **12c** lead to (R)-enantiomers.

Due to the fact that **12c** and **12d** lead to the most favorable transition states for the (R) and (S) products, respectively, only the pathways starting from **12c** and **12d** are presented in Fig. 4a for simplicity. With the assistance of the alkoxy anion ligand, **12c** undergoes a facile hydride transfer from the Bpin group to the carbonyl group, affording the R-configured **14c** with an activation barrier of 12.9 kcal/mol (via **TS-12c-14c**). From **14c**, a two-stage Al-O/O-B σ-bond metathesis yields the Al-hydroboration product complex **16c** via a transfer of the Bpin group. During the first stage, a B-O bond is formed between the Bpin group and the alkoxy anion ligand in **14c** (via **TS-14c-15c**), resulting in an Al-O-B-O four-membered ring intermediate **15c**. Then, **15c** undergoes the dissociation of the old B-O bond (via **TS-15c-16c**), forming the complex **16c**. Finally, **16c** releases the hydroboration product **(R)-2a** and regenerates aluminum complex **12c** through ligand exchange. Aluminum species **12d** is responsible for the formation of the S-configured product and the key hydride transfer process requires an activation barrier of 21.2 kcal/mol via **TS-12d-15d**. It is worth mentioning that although the absolute configurations of the chiral aluminum center in **12c** and **12d** are both Λ, the exposed prochiral surfaces of bidentate coordinated substrates in these two configurations are opposite, so they will yield products with opposite configurations. The barrier difference between **TS-12c-14c** and **TS-12d-15d** is predicted to be 8.4 kcal/mol using B3LYP-D3 method. We have also calculated the free energy barriers for four different transition states starting from **12a**–**12d** using highly accurate DLPNO-CCSD(T) method. The absolute errors between the B3LYP-D3 and DLPNO-CCSD(T) free energy barriers are always less than 1.0 kcal/mol (Supplementary Table 3). For the barrier difference between **TS-12c-14c** and **TS-12d-15d**, the DLPNO-CCSD(T) method predicted a value of 8.3 kcal/mol, which is close to the B3LYP-D3 result. The calculated $\Delta\Delta G^{\ddagger}$ values are in qualitative consistency with the experimentally observed enantioselectivity (99% ee).

Besides regenerating catalytically active species through Al-O/O-B σ-bond metathesis and then ligand exchange, **14c** can directly undergo ligand exchange with substrate **1a** to give the hexacoordinated aluminum species with similar catalytic activity, such as **17c** and **17d** (Supplementary Figs. 8 and 9). As shown in Fig. 4b, as a species like **12c**, intermediate **17c** can also undergo ligand-assisted hydroboration reaction with HBpin affording (R)-configurated product, with a lower activation barrier (via **TS-17c-18c**, $\Delta G^{\ddagger}$ = 10.9 kcal/mol). The reaction of **17d** with HBpin generates (S)-configurated product just like **12d**. Given the similar coordination geometry, the activation barrier difference in the stereo-determining step for the hydroboration with **17c**/**17d** ($\Delta\Delta G^{\ddagger}$ = 8.0 kcal/mol) is close to that of **12c** and **12d** ($\Delta\Delta G^{\ddagger}$ = 8.4 kcal/mol).

The hexacoordinated aluminum alkoxides-based mechanism successfully explained the enantioselectivity with **1a** as the substrate in the preceding section. We then investigated whether this mechanism can also account for the asymmetric hydroboration of diaryl substrates. With 2-benzoylpyridine **1b** as the substrate, similar hexacoordinated aluminum alkoxides species (**20a**–**20h, 23a**–**23h**) and

https://doi.org/10.1038/s41467-025-56000-y

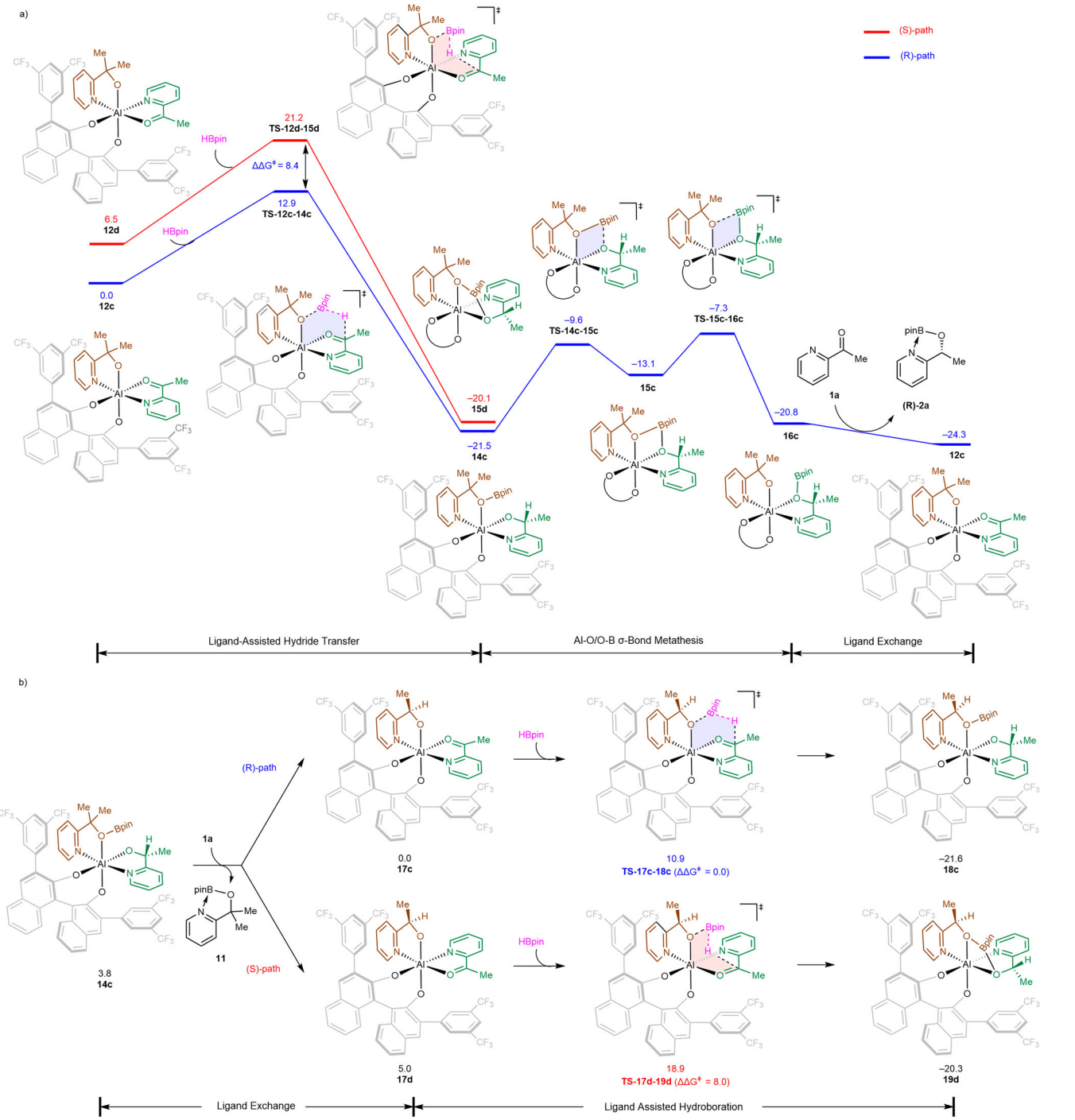


**Fig. 4 | Octahedral chiral-at-aluminum catalysis. a** Free energy profile for the hexacoordinated aluminum alkoxides **12c**/**12d** (with α,α-dimethyl-2-pyridyl alkoxide as one of the ligands) catalyzed hydroboration. **b** Free energy profile for the **17c**/**17d** (with α-methyl-2-pyridyl alkoxide as one of the ligands) catalyzed hydroboration. Gibbs free energies are in kcal/mol with respect to **12c** or **17c**. Computational details are described in the text.

their hydride transfer transition states have also been computationally located (Fig. 5 and Supplementary Figs. 10–13). Similarly, species **20c** and **23c** are the most stable configurations among all the configurations considered. Starting from **20c** or **23c**, the formation of the major R-enantiomer is energetically more favorable with activation barriers of 13.3 kcal/mol (via **TS-20c-21c)** and 10.7 kcal/mol (via **TS-23c-24c**). The pathway to yield the S-enantiomer involves much higher barriers (23.5 kcal/mol via **TS-20d-22d**, or 18.7 kcal/mol via **TS-23d-25d**), respectively. Unlike the originally proposed Al-H mechanism, the hexacoordinated aluminum alkoxides-based mechanism can account for the experimentally observed enantioselectivity (99% ee) for diaryl substrates.

## Theoretical investigation on the asymmetric induction mechanism

With the favored activation mode established, we then investigated the factors affecting the enantioselectivity. We decomposed the free energy barrier difference ($\Delta\Delta G_{Rel}^{\ddagger}$) of the stereo-determining step into the contributions of stability difference of the related hexacoordinated aluminum intermediates ($\Delta\Delta G_{Int}$) and intrinsic energy difference of the

https://doi.org/10.1038/s41467-025-56000-y

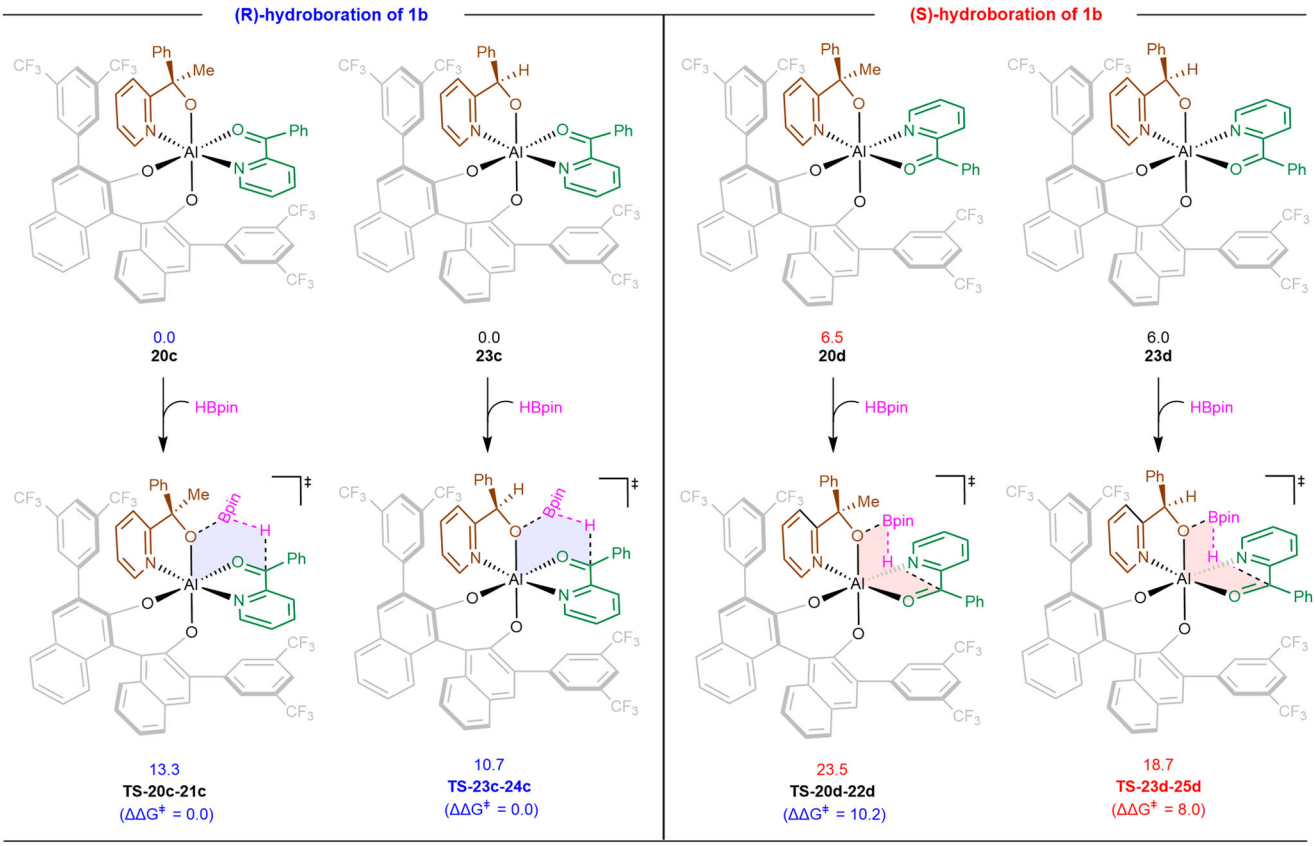


**Fig. 5 | Key intermediates and transition states involved in hydroboration of 2-benzoylpyridine 1b.** Gibbs free energies are in kcal/mol with respect to **20c** and **23c**. Computational details are described in the text. Hexacoordinated aluminum alkoxides **23c** and **23d** with a secondary alkoxy ligand are generated through ligand exchange (see Supplementary Fig. 13 for ligand exchange step).

a)

| Substrate | Reactive Species | $\Delta\Delta G_{Int}$ | $\Delta\Delta G_{Intri}^{\ddagger}$ | $\Delta\Delta G_{Rel}^{\ddagger}$ | Exp. ee |
|---|---|---|---|---|---|
| **1a** 2-acetylpyridine | **12c/12d** | 6.5 | 1.9 | 8.4 | 99% |
| | **17c/17d** | 5.0 | 3.0 | 8.0 | |
| **1b** 2-benzoylpyridine | **20c/20d** | 6.5 | 3.7 | 10.2 | 99% |
| | **23c/23d** | 6.0 | 2.0 | 8.0 | |

$\Delta\Delta G_{Intri}^{\ddagger} = \Delta\Delta G_{Rel}^{\ddagger} - \Delta\Delta G_{Int}$, in kcal/mol.

b)

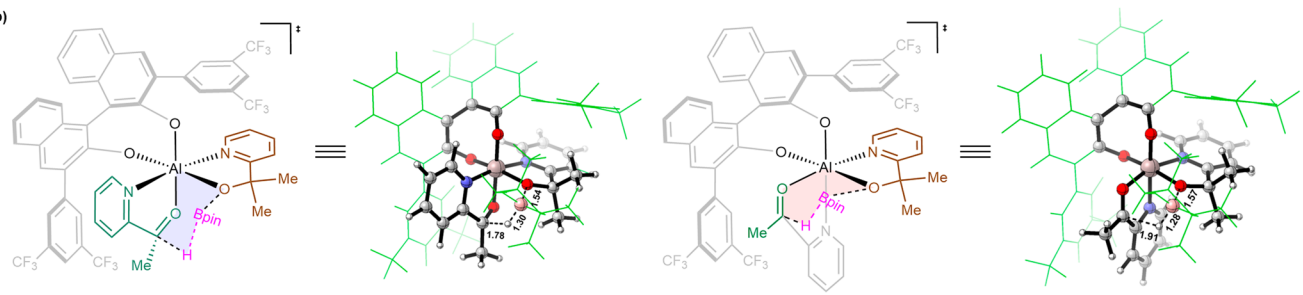


**Fig. 6 | Origin of enantioselectivity. a** Contributions of free energy barrier difference ($\Delta\Delta G_{Rel}^{\ddagger}$) in the stereo-determining step and the experimental ee values with isolated species **13g** as the catalyst. Gibbs free energies are in kcal/mol with respect to **12c**, **17c**, **20c** and **23c**. Computational details are described in the text. **b** Structural characteristics of the key hydride transfer transition states **TS-12c-14c** and **TS-12d-15d**. Distances are in angstroms (Å). Color codes: H, white; B, pink; C, gray; O, red; N, blue; Al, dusty pink.

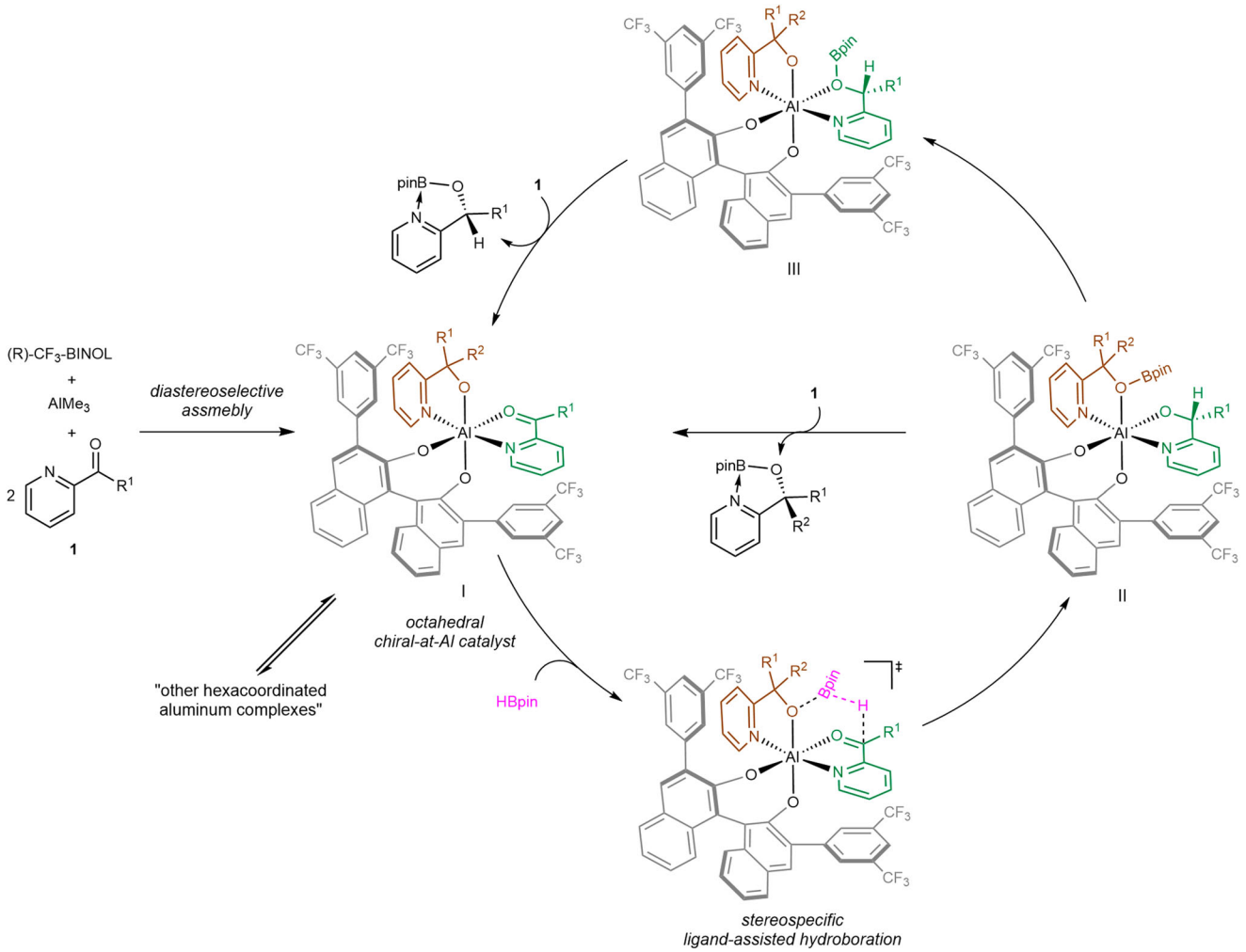


**Fig. 7 | Proposed chiral-at-aluminum mechanism for the BINOL-aluminum-catalyzed asymmetric hydroboration of heteroaryl ketones.** $R^1$ = alkyl, aryl group; $R^2$ = Me or H.

related transition states ($\Delta\Delta G_{Intri}^{\ddagger} = \Delta\Delta G_{Rel}^{\ddagger} - \Delta\Delta G_{Int}$, Fig. 6a). Interestingly, $\Delta\Delta G_{Int}$ contributes more than a half to the free energy barrier difference. This means that the source of enantioselectivity is largely a preference for the arrangement of different coordination species at the aluminum center. In addition, $\Delta\Delta G_{Intri}^{\ddagger}$ also contributes to the free energy barrier difference in the stereo-determining step. For **TS-12c-14c** related to the formation of major R-enantiomer, this six-membered transition state adopts a chair conformation (Fig. 6b). In contrast, **TS-12d-15d** adopts a boat-like geometry. This conformational difference was proposed to be responsible for the calculated $\Delta\Delta G_{Intri}^{\ddagger}$.

Previously, the steric hindrance between the side arms of BINOL ligands and the substrates was proposed to be vital for stereoinduction[15,42]. However, in the current favored reaction mode, the substrates are arranged in parallel with the side arms of BINOL, resulting in little steric hindrance effect. The observed enantioselectivity is determined by the aluminum-centered chirality resulting from the assembly mode of the substrates around the aluminum center. Accordingly, the chirality transfer mechanism is from chiral ligand to aluminum-centered chirality, and then to the final hydroboration product. For this reason, this reaction mode can account for the enantioselectivity observed with diaryl 2-benzoylpyridine **1b** as the substrate, a case for which the Al-H based mechanism was unable to explain the results.

Based on our computational and experimental studies, we proposed an octahedral aluminum-based mechanism for the BINOL-aluminum-catalyzed asymmetric hydroboration of heteroaryl ketones (Fig. 7). The diastereoselective assembly of in situ generated [(R)-$CF_3$-BINOL-AlMe]$_2$ species with two equivalents of substrates yields hexacoordinated aluminum alkoxide that is the catalytically relevant species **I**. In the solution phase, **I** is in coexistence with some other hexacoordinated aluminum complexes. Subsequently, species **I** undergoes stereo-determining ligand-assisted hydride transfer to generate the hydroalumination intermediate **II**. The aluminum-centered chirality induced by the chiral BINOL ligand leads to the experimentally observed enantioselectivity. **II** can undergo Al-O/O-B σ-bond metathesis, leading to **III**. The subsequent ligand exchange regenerates the hexacoordinated aluminum alkoxide **I** and liberates the desired product. Besides, intermediate **II** can also directly undergo ligand exchange with another substrate molecule to regenerate the related hexacoordinated aluminum complex **I** and liberate the chiral hydroboration product. The alkoxy anionic ligand plays an important role in the catalytic cycle. First, the complexation of the anionic ligand with the Bpin group enhances the nucleophilic attack of the hydride on the carbon atom of the carbonyl group. In addition, the anionic ligand acts as a relay for the transfer of the Bpin group to the oxygen atom of the carbonyl group in the Al-O/O-B σ-bond metathesis step.

## Discussion

In summary, we have identified an octahedral chiral-at-aluminum catalysis mechanism in BINOL-aluminum-catalyzed asymmetric

hydroboration of heteroaryl ketones. BINOL-induced diastereoselective assembly leads to the catalytically active hexacoordinated aluminum alkoxides and determines the absolute configuration of the product. The predicted hexacoordinated aluminum complex was successfully isolated and characterized by single-crystal X-ray diffraction analysis. Further experiments identified the catalytic reactivity of this discovered aluminum complex. This work demonstrated that the combination of main-group metals and simple BINOL ligands can be assembled into chiral-at-metal complexes in the presence of bidentate substrates. In these complexes, the substrates might be activated through a LUMO activation mode[3,68] and the alkoxy anionic ligand could be noninnocent, as discussed in the preceding section. We expect our present work to stimulate the future development of asymmetric catalysis using main-group aluminum catalysts, as well as the design of other asymmetric reactions based on the BINOL/metal combination.

## Methods

### Computational methods

All density functional calculations were performed with the Gaussian 16 package (Revision A.03)[69]. Geometry optimizations and vibrational frequency analysis were performed at B3LYP[53,54]-D3[55]/Def2-SVP level. The solvent effect was dealed with polarizable continuum model (PCM)[56,57] in toluene or dichloromethane. The Def2-TZVP basis set was used to get more accurate single-point energies for all structures with the same functional and implicit solvent model. To simulate ECD spectra, TD-DFT calculations with 100 considered excited state were carried out at B3LYP-D3/Def2-TZVP level with the PCM model to deal with the solvent effect of dichloromethane. DLPNO-CCSD(T)[59] calculations with Def2-TZVP basis set were performed with ORCA 5.0[70] software.

### Procedure for the synthesis of hexacoordinated aluminum alkoxides 13g

Inside a glovebox under argon atmosphere, to a solution of (R)-$CF_3$-BINOL (284.2 mg, 0.4 mmol) in dichloromethane (1.6 mL), $AlMe_3$ (0.4 mmol, 200 μL, 2 M in toluene) was dropwise added. After the gas stopped releasing, the reaction solution was stirred at room temperature for 3 h. The in situ generated [(R)-$CF_3$-BINOL-AlMe]$_2$ was dropwise added to a solution of (4-chlorophenyl)(pyridin-2-yl)methanone **1c** (174.1 mg, 0.8 mmol) in dichloromethane (1.6 mL). The reaction solution was then stirred at room temperature for 2 h. Through a filter membrane, the reaction solution was equally filtered into four small test tubes (inner diameter 6 mm, length 20 cm). To each small test tube, 0.1 mL of dichloromethane was added as a buffer layer. Then each small test tube was layered with at least 1.3 mL of pentane as poor solvent. Finally, the test tubes were tightly sealed. After standing for two weeks, red block crystals of **13g** grew on the test tube wall as the sole solids. The mother liquor was decanted off and the solid was washed with cold pentane, affording the product in a yield of 31% (147 mg).

## Data availability

All data that support the findings of this study are available within the paper and its supplementary information files, and also available from the corresponding author upon request. The X-ray crystallographic structures data generated in this study have been deposited in the Cambridge Crystallographic Data Center (CCDC) database under accession code 2288118, 2288119, and 2309175, and can be obtained free of charge via www.ccdc.cam.ac.uk. The xyz coordinates of the optimized structures in this study are provided in the Source Data file. Source data are provided with this paper.

## References


1. Yoon, T. P. & Jacobsen, E. N. Privileged chiral catalysts. *Science* **299**, 1691–1693 (2003).
2. Zhou, Q.-L. Privileged chiral ligands and catalysts. (Wiley-VCH, Weinheim; 2011).
3. Liu, X., Zheng, H., Xia, Y., Lin, L. & Feng, X. Asymmetric cycloaddition and cyclization reactions catalyzed by chiral N,N′-dioxide–metal complexes. *Acc. Chem. Res.* **50**, 2621–2631 (2017).
4. Yamakawa, M., Ito, H. & Noyori, R. The metal–ligand bifunctional catalysis: a theoretical study on the ruthenium(ii)-catalyzed hydrogen transfer between alcohols and carbonyl compounds. *J. Am. Chem. Soc.* **122**, 1466–1478 (2000).
5. Allemann, C., Gordillo, R., Clemente, F. R., Cheong, P. H.-Y. & Houk, K. N. Theory of asymmetric organocatalysis of aldol and related reactions: rationalizations and predictions. *Acc. Chem. Res.* **37**, 558–569 (2004).
6. Taylor, M. S. & Jacobsen, E. N. Asymmetric catalysis by chiral hydrogen-bond donors. *Angew. Chem. Int. Ed.* **45**, 1520–1543 (2006).
7. Mitsumori, S. et al. Direct asymmetric anti-mannich-type reactions catalyzed by a designed amino acid. *J. Am. Chem. Soc.* **128**, 1040–1041 (2006).
8. Houk, K. N. & Cheong, P. H.-Y. Computational prediction of small-molecule catalysts. *Nature* **455**, 309–313 (2008).
9. Wheeler, S. E., Seguin, T. J., Guan, Y. & Doney, A. C. Noncovalent interactions in organocatalysis and the prospect of computational catalyst design. *Acc. Chem. Res.* **49**, 1061–1069 (2016).
10. Poree, C. & Schoenebeck, F. A holy grail in chemistry: computational catalyst design: feasible or fiction? *Acc. Chem. Res.* **50**, 605–608 (2017).
11. Chen, Y., Yekta, S. & Yudin, A. K. Modified BINOL ligands in asymmetric catalysis. *Chem. Rev.* **103**, 3155–3212 (2003).
12. Brunel, J. M. BINOL: a versatile chiral reagent. *Chem. Rev.* **105**, 857–898 (2005).
13. Shibasaki, M. & Matsunaga, S. Design and application of linked-BINOL chiral ligands in bifunctional asymmetric catalysis. *Chem. Soc. Rev.* **35**, 269–279 (2006).
14. Pu, L. Asymmetric functional organozinc additions to aldehydes catalyzed by 1,1′-Bi-2-naphthols (BINOLs). *Acc. Chem. Res.* **47**, 1523–1535 (2014).
15. Cohen, R., Graves, C. R., Nguyen, S. T., Martin, J. M. L. & Ratner, M. A. The mechanism of aluminum-catalyzed Meerwein–Schmidt–Ponndorf–Verley reduction of carbonyls to alcohols. *J. Am. Chem. Soc.* **126**, 14796–14803 (2004).
16. Hamashima, Y., Sawada, D., Kanai, M. & Shibasaki, M. A new bifunctional asymmetric catalysis: an efficient catalytic asymmetric cyanosilylation of aldehydes. *J. Am. Chem. Soc.* **121**, 2641–2642 (1999).
17. Cho, B. T. Recent development and improvement for boron hydride-based catalytic asymmetric reduction of unsymmetrical ketones. *Chem. Soc. Rev.* **38**, 443–452 (2009).
18. Wang, R. & Park, S. Recent advances in metal-catalyzed asymmetric hydroboration of ketones. *ChemCatChem* **13**, 1898–1919 (2021).
19. Guo, J., Chen, J. & Lu, Z. Cobalt-catalyzed asymmetric hydroboration of aryl ketones with pinacolborane. *Chem. Commun.* **51**, 5725–5727 (2015).
20. Chen, F., Zhang, Y., Yu, L. & Zhu, S. Enantioselective NiH/pmrox-catalyzed 1,2-reduction of α,β-unsaturated ketones. *Angew. Chem. Int. Ed.* **56**, 2022–2025 (2017).
21. Vasilenko, V., Blasius, C. K., Wadepohl, H. & Gade, L. H. Mechanism-based enantiodivergence in manganese reduction catalysis: a chiral pincer complex for the highly enantioselective hydroboration of ketones. *Angew. Chem. Int. Ed.* **56**, 8393–8397 (2017).
22. Chen, S. et al. Tris(cyclopentadienyl)lanthanide complexes as catalysts for hydroboration reaction toward aldehydes and ketones. *Org. Lett.* **19**, 3382–3385 (2017).

23. Song, P., Lu, C., Fei, Z., Zhao, B. & Yao, Y. Enantioselective reduction of ketones catalyzed by rare-earth metals complexed with phenoxy modified chiral prolinols. *J. Org. Chem.* **83**, 6093–6100 (2018).
24. Sun, Y., Lu, C., Zhao, B. & Xue, M. Enantioselective hydroboration of ketones catalyzed by rare-earth metal complexes containing trost ligands. *J. Org. Chem.* **85**, 10504–10513 (2020).
25. Power, P. P. Main-group elements as transition metals. *Nature* **463**, 171–177 (2010).
26. Stephan, D. W. & Erker, G. Frustrated lewis pairs: metal-free hydrogen activation and more. *Angew. Chem. Int. Ed.* **49**, 46–76 (2010).
27. Egorova, K. S. & Ananikov, V. P. Which metals are green for catalysis? Comparison of the toxicities of Ni, Cu, Fe, Pd, Pt, Rh, and Au salts. *Angew. Chem. Int. Ed.* **55**, 12150–12162 (2016).
28. Wilkins, L. C. & Melen, R. L. Enantioselective main group catalysis: modern catalysts for organic transformations. *Coord. Chem. Rev.* **324**, 123–139 (2016).
29. Yang, Z. et al. An aluminum hydride that functions like a transition-metal catalyst. *Angew. Chem. Int. Ed.* **54**, 10225–10229 (2015).
30. Jakhar, V. K., Barman, M. K. & Nembenna, S. Aluminum monohydride catalyzed selective hydroboration of carbonyl compounds. *Org. Lett.* **18**, 4710–4713 (2016).
31. Pollard, V. A. et al. Lithium diamidodihydridoaluminates: bimetallic cooperativity in catalytic hydroboration and metallation applications. *Chem. Commun.* **54**, 1233–1236 (2018).
32. Bismuto, A., Cowley, M. J. & Thomas, S. P. Aluminum-catalyzed hydroboration of alkenes. *ACS Catal.* **8**, 2001–2005 (2018).
33. Yadav, S., Pahar, S. & Sen, S. S. Benz-amidinato calcium iodide catalyzed aldehyde and ketone hydroboration with unprecedented functional group tolerance. *Chem. Commun.* **53**, 4562–4564 (2017).
34. Jin, D., Sun, X. & Roesky, P. W. Heavy alkaline–earth metal formazanate complexes and their catalytic applications. *Organometallics* **42**, 1725–1731 (2023).
35. Arrowsmith, M., Hadlington, T. J., Hill, M. S. & Kociok-Köhn, G. Magnesium-catalysed hydroboration of aldehydes and ketones. *Chem. Commun.* **48**, 4567–4569 (2012).
36. Jang, Y. K., Magre, M. & Rueping, M. Chemoselective luche-type reduction of α,β-unsaturated ketones by magnesium catalysis. *Org. Lett.* **21**, 8349–8352 (2019).
37. Lawson, J. R., Wilkins, L. C. & Melen, R. L. Tris(2,4,6-trifluorophenyl) borane: an efficient hydroboration catalyst. *Chem. Eur. J.* **23**, 10997–11000 (2017).
38. Corey, E. J. & Helal, C. J. Reduction of carbonyl compounds with chiral oxazaborolidine catalysts: a new paradigm for enantioselective catalysis and a powerful new synthetic method. *Angew. Chem. Int. Ed.* **37**, 1986–2012 (1998).
39. Falconnet, A., Magre, M., Maity, B., Cavallo, L. & Rueping, M. Asymmetric magnesium-catalyzed hydroboration by metal-ligand cooperative catalysis. *Angew. Chem. Int. Ed.* **58**, 17567–17571 (2019).
40. Titze, M., Heitkämper, J., Junge, T., Kästner, J. & Peters, R. Highly active cooperative lewis acid—ammonium salt catalyst for the enantioselective hydroboration of ketones. *Angew. Chem. Int. Ed.* **60**, 5544–5553 (2021).
41. Nicholson, K. et al. A boron–oxygen transborylation strategy for a catalytic midland reduction. *ACS Catal.* **11**, 2034–2040 (2021).
42. Lebedev, Y. et al. Asymmetric hydroboration of heteroaryl ketones by aluminum catalysis. *J. Am. Chem. Soc.* **141**, 19415–19423 (2019).
43. Chavarot, M. et al. Chiral-at-Metal" octahedral ruthenium(II) complexes with achiral ligands: a new type of enantioselective catalyst. *Inorg. Chem.* **42**, 4810–4816 (2003).
44. Belokon, Y. N. et al. Asymmetric synthesis of cyanohydrins catalysed by a potassium Δ-bis[N-salicylidene-(R)-tryptophanato] cobaltate complex. *Mendeleev Commun.* **14**, 249–250 (2004).
45. Abell, J. P. & Yamamoto, H. Development and applications of tethered bis(8-quinolinolato) metal complexes (TBOxM). *Chem. Soc. Rev.* **39**, 61–69 (2010).
46. Chen, L.-A. et al. Chiral-at-metal octahedral iridium catalyst for the asymmetric construction of an all-carbon quaternary stereocenter. *Angew. Chem. Int. Ed.* **52**, 14021–14025 (2013).
47. Cruchter, T. & Larionov, V. A. Asymmetric catalysis with octahedral stereogenic-at-metal complexes featuring chiral ligands. *Coord. Chem. Rev.* **376**, 95–113 (2018).
48. Vasilenko, V., Blasius, C. K. & Gade, L. H. One-pot sequential kinetic profiling of a highly reactive manganese catalyst for ketone hydroboration: leveraging σ-bond metathesis via alkoxide exchange steps. *J. Am. Chem. Soc.* **140**, 9244–9254 (2018).
49. Rothbaum, J. O., Motta, A., Kratish, Y. & Marks, T. J. Mechanistic study of homoleptic trisamidolanthanide-catalyzed aldehyde and ketone hydroboration. Chemically non-innocent ligand participation. *Chem. Sci.* **14**, 3247–3256 (2023).
50. Campbell, E. J., Zhou, H. & Nguyen, S. T. The asymmetric Meerwein–Schmidt–Ponndorf–Verley reduction of prochiral ketones with iPrOH catalyzed by Al catalysts. *Angew. Chem. Int. Ed.* **41**, 1020–1022 (2002).
51. Graves, C. R., Zhou, H., Stern, C. L. & Nguyen, S. T. A mechanistic investigation of the asymmetric Meerwein–Schmidt–Ponndorf –Verley Reduction Catalyzed by BINOL/AlMe3 structure, kinetics, and enantioselectivity. *J. Org. Chem.* **72**, 9121–9133 (2007).
52. Zheng, L. et al. Asymmetric catalytic Meerwein–Ponndorf–verley reduction of ketones with aluminum(III)-VANOL catalysts. *ACS Catal* **10**, 7188–7194 (2020).
53. Becke, A. D. Density-functional exchange-energy approximation with correct asymptotic behavior. *Phys. Rev. A* **38**, 3098–3100 (1988).
54. Lee, C., Yang, W. & Parr, R. G. Development of the Colle-Salvetti correlation-energy formula into a functional of the electron density. *Phys. Rev. B* **37**, 785–789 (1988).
55. Grimme, S., Antony, J., Ehrlich, S. & Krieg, H. A consistent and accurate ab initio parametrization of density functional dispersion correction (DFT-D) for the 94 elements H-Pu. *J. Chem. Phys.* **132**, 154104–154122 (2010).
56. Scalmani, G. & Frisch, M. J. Continuous surface charge polarizable continuum models of solvation. I. General formalism. *J. Chem. Phys.* **132**, 114110–114124 (2010).
57. Tomasi, J., Mennucci, B. & Cammi, R. Quantum mechanical continuum solvation models. *Chem. Rev.* **105**, 2999–3094 (2005).
58. Zhang, L. & Meggers, E. Steering asymmetric lewis acid catalysis exclusively with octahedral metal-centered chirality. *Acc. Chem. Res.* **50**, 320–330 (2017).
59. Guo, Y. et al. Communication: an improved linear scaling perturbative triples correction for the domain based local pair-natural orbital based singles and doubles coupled cluster method DLPNO-CCSD(T). *J. Chem. Phys.* **148**, 11101–11105 (2018).
60. Lefebvre, C. et al. Accurately extracting the signature of intermolecular interactions present in the NCI plot of the reduced density gradient versus electron density. *Phys. Chem. Chem. Phys.* **19**, 17928–17936 (2017).
61. Lu, T. & Chen, F. Multiwfn: a multifunctional wavefunction analyzer. *J. Comput. Chem.* **33**, 580–592 (2012).
62. Quagliano, J. V. & Schubert, L. E. O. The trans effect in complex inorganic compounds. *Chem. Rev.* **50**, 201–260 (1952).
63. Hartley, F. R. The cis- and trans-effects of ligands. *Chem. Soc. Rev.* **2**, 163–179 (1973).
64. Son, A. J. R., Thorn, M. G., Fanwick, P. E. & Rothwell, I. P. Isolation and chemistry of aluminum compounds containing (S)-3,3′-Bis(triphenylsilyl)-1,1′-bi-2,2′-naphthoxide ligands. *Organometallics* **22**, 2318–2324 (2003).

65. Ooi, T., Ichikawa, H. & Maruoka, K. Practical approach to the Meerwein–Ponndorf–Verley reduction of carbonyl substrates with new aluminum catalysts. *Angew. Chem. Int. Ed.* **40**, 3610–3612 (2001).
66. Yang, M., Zou, J., Wang, G. & Li, S. Automatic reaction pathway search via combined molecular dynamics and coordinate driving method. *J. Phys. Chem. A* **121**, 1351–1361 (2017).
67. Li, G. et al. Combined molecular dynamics and coordinate driving method for automatically searching complicated reaction pathways. *Phys. Chem. Chem. Phys.* **25**, 23696–23707 (2023).
68. Houk, K. N. Frontier molecular orbital theory of cycloaddition reactions. *Acc. Chem. Res.* **8**, 361–369 (1975).
69. Frisch, M.J. et al. Gaussian 16 Rev. A.03. (Wallingford, CT; 2016).
70. Neese, F. Software update: the ORCA program system—version 5.0. *WIREs Comput. Mol. Sci.* **12**, e1606 (2022).

## Acknowledgements

This work was supported by National Natural Science Foundation of China (Nos. 22073043 from S.H.L., and 22273035 from G.Q.W.), the New Cornerstone Science Foundation (S.H.L.), the Fundamental Research Funds for the Central Universities (No. 020514380295, G.Q.W.), and Graduate Student Scientific Research Innovation Projects in Jiangsu Province (No. KYCX23_0111, Z.X.L.). We thank Dr. Jia Cao and Dr. Hui Chen for their insightful discussions. We acknowledge Prof. Juli Jiang for her help on ECD experiments. We acknowledge Prof. Xu Cheng and Prof. Wenhua Zheng for their help on HPLC experiments. We thank Prof. Jianjun Feng for his help on the experiments. All theoretical calculations were performed at the High-Performance Computing Center (HPCC) of Nanjing University.

## Author contributions

Z.X.L., G.Q.W. and S.H.L conceived the work and designed the computational and experimental investigations. Z.X.L. performed the DFT calculations. Z.G.N. analyzed the non-covalent interactions and performed the DLPNO-CCSD(T) calculations. Z.X.L., P.F.C., L.Z.G. and C.Q.Z. conducted the isolation of catalytically active species. Y.Z. analyzed the single crystal structures. R.R.W performed the ECD experiments. Z.X.L. conducted catalytic performance validation of the isolated aluminum species. Z.X.L. and G.Q.W. co-wrote the manuscript with the input from all the other authors. G.Q.W. and S.H.L. directed the project.

## Competing interests

The authors declare no competing interests.

## Additional information

**Supplementary information** The online version contains supplementary material available at https://doi.org/10.1038/s41467-025-56000-y.

**Correspondence** and requests for materials should be addressed to Guoqiang Wang or Shuhua Li.

**Peer review information** *Nature Communications* thanks Xiaoli Ma and the other, anonymous, reviewer(s) for their contribution to the peer review of this work. A peer review file is available.